

Explainable AI with counterfactual paths

Bastian Pfeifer¹, Mateusz Krzyzinski², Hubert Baniecki³, Anna Saranti^{1,4},
Andreas Holzinger^{1,4}, and Przemyslaw Biecek^{2,3}

¹ Institute for Medical Informatics, Statistics and Documentation.
Medical University Graz, Austria
`bastian.pfeifer@medunigraz.at`

² MI2.AI, Warsaw University of Technology, Poland

³ MI2.AI, University of Warsaw, Poland

⁴ Human-Centered AI Lab, University of Natural Resources and Life Sciences,
Vienna, Austria

Abstract. Explainable AI (XAI) is an increasingly important area of research in machine learning, which in principle aims to make black-box models transparent and interpretable. In this paper, we propose a novel approach to XAI that uses counterfactual paths generated by conditional permutations. Our method provides counterfactual explanations by identifying alternative paths that could have led to different outcomes. The proposed method is particularly suitable for generating explanations based on counterfactual paths in knowledge graphs. By examining hypothetical changes to the input data in the knowledge graph, we can systematically validate the behaviour of the model and examine the features or combination of features that are most important to the model's predictions. Our approach provides a more intuitive and interpretable explanation for the model's behaviour than traditional feature weighting methods and can help identify and mitigate biases in the model.

Keywords: explainable AI, knowledge graph, feature importance, counterfactual explanation

1 Introduction

The field of Artificial Intelligence (AI) has made significant strides in recent years, with the development of advanced machine learning algorithms that can accurately predict outcomes and make decisions. However, these algorithms are often viewed as "black boxes" that provide little insight into their decision-making processes, leading to concerns about their fairness, accountability, and transparency. This lack of transparency is particularly problematic when AI is used in critical applications such as healthcare, finance, and criminal justice.

Explainable AI (XAI) has emerged as a promising solution to this problem by providing human-understandable explanations of AI decision-making. One approach to XAI is through the use of counterfactual explanations, which involve generating alternative scenarios that could have led to different outcomes.

Counterfactual explanations can help users understand how an AI model arrived at a particular decision and what factors influenced that decision.

Counterfactual paths represent the relationships between input features and the output of the model, allowing users to explore how changing individual features or combinations of features affect the model’s output. One of the main advantages of counterfactual paths is their ability to provide insights into how the model works and to identify potential biases or confounding factors that may affect its predictions. These insights can be used to improve the model’s accuracy, fairness, and robustness.

Furthermore, counterfactual paths could provide a more intuitive and interpretable explanation of the model’s behaviour than traditional feature importance methods. For example, rather than simply providing a list of the top features that contribute to the model’s predictions, counterfactual paths can show how changes to specific combination of features lead to changes in the output of the model. This can help users to better understand the underlying patterns in the data and the behaviour of the model.

In this paper, we introduce the CPATH algorithm for model-agnostic global explanations using counterfactual paths. Compared to classical feature attribution methods, CPATH provides more intuitive, interpretable, and graphical explanations and thus can help to uncover the decisions made by black-box models.

2 Related work

Model-agnostic feature importance. Explaining a predictive model on a *global* level aims to understand how important is a given feature to its performance. Several model-agnostic, i.e. explaining any black-box function, feature importance measures have been proposed. The widely adopted approach is permutation feature importance (Fisher et al., 2019), which is also extended to local and partial importance (Casalicchio et al., 2019). Molnar et al. (2021) introduce confidence intervals for permutation feature importance and Au et al. (2022) propose to group features to explain their combined importance. In practice, estimating the marginal importance of a single feature without taking into account correlation structure in data is a challenge (Molnar et al., 2023). To address feature dependence, Watson and Wright (2021) proposes to measure the conditional predictive impact between features and predictions using the knockoff sampling framework; also for categorical features (Blesch et al., 2023). Related is work on conditional estimation of Shapley-based feature attributions Aas et al. (2021). As opposed to considering Shapley-based feature importance measures (Casalicchio et al., 2019; Covert et al., 2020), in this paper, we specifically relate permutation importance to counterfactual explanations.

Counterfactual explanations. A counterfactual explanation of model prediction describes the smallest change to the feature values that change the predicted class. It is a useful *local* “what-if” explanation for making actionable decisions

Wachter et al. (2017). One can optimize to find counterfactuals using model-specific optimization methods, e.g. gradients. Our work relates more to model-agnostic approaches available to any black-box model (Karimi et al., 2020). Dandl et al. (2020) propose multi-objective counterfactual explanations that take into account data manifold, i.e. how likely it is that the counterfactual data point originates from the training data distribution. Mothilal et al. (2020) focus on finding a diverse set of counterfactual data points for a given prediction. Most recent work considers the robustness of such explanations to (potentially adversarial) data perturbations (Pawelczyk et al., 2023). Contrary to related work, we use the intuition behind counterfactual explanations to construct a novel global explanation of feature importance.

Domain knowledge in the context of model explanation. Relating explanations to domain knowledge is an emerging research topic (Biecek and Burzykowski, 2021). Crucially, interpreting models should be done with respect to data distribution and its correlation structure (Baniecki et al., 2023; Molnar et al., 2021). One idea is to build a surrogate model based on explanations of a black-box function achieving an interpretable predictive interface consistent with domain knowledge (Alaa et al., 2021; Gosiewska et al., 2021). Other approaches consider including domain knowledge directly in the algorithm used to learn a predictive function (Confalonieri et al., 2021; Panigutti et al., 2020; Pfeifer et al., 2022a), which is challenging to do in an algorithm-agnostic way.

In this paper, we introduce feature importance explanation and visualization through counterfactual paths that provide additional information about the graph structure of features. Domain knowledge can both be derived from explanations, as well as participate in estimating more accurate explanations.

3 Counterfactual paths for explaining black-box models

3.1 Intuition

The herein proposed CPATH algorithm randomly selects paths through the feature space, where each feature represents a node in a fully-connected graph or a knowledge graph, masking the sampling scheme. Once a path is created, CPATH permutes one feature after the other of the sampled path and terminates as soon as a certain number of class labels swap to the inverse class. We call these paths *counterfactual paths*. From these counterfactual paths, we derive an adjacency matrix weighted by the inferred path lengths. Based on the weighted adjacency matrix the *global* importance of a certain feature is determined.

3.2 Mathematical formulation

Let $\mathcal{M}: \mathbb{R}^p \rightarrow \{1, \dots, g\}$, where g is the number of classes, denote the model of interest, which is a classifier. Given an observation $\mathbf{x} = (x_1, x_2, \dots, x_p) \in \mathbb{R}^p$, the model's prediction is denoted as $\mathcal{M}(\mathbf{x})$.

We describe the problem using weighted directed graphs, (weighted digraphs). A graph $G_{\mathcal{M}} = (V, E, w_{\mathcal{M}})$ is defined as an ordered triple, where $V = 1, \dots, p$ represents the set of predictors (explanatory variables) that form the vertices of the graph. The set of directed edges (arcs), denoted as E , contains ordered pairs of vertices (i, j) such that there exists a directed edge from vertex i to vertex j . The function $w_{\mathcal{M}}: E \rightarrow \mathbb{R}$ maps the edges to their weights and can also be represented as an adjacency matrix W .

The variables used in the \mathcal{M} model which constitute the set of vertices V are predetermined, i.e., these are the variables used in the model fitting process. Similarly, the set E is known – its form can be derived from a domain knowledge graph describing the process of generating the data. However, if the domain knowledge graph is unknown, it can be assumed that $G_{\mathcal{M}}$ is a complete digraph, meaning that each pair of vertices is connected by a symmetric pair of directed arcs.

The objective is to estimate the function $w_{\mathcal{M}}$ (related to the adjacency matrix W) by aggregating *counterfactual paths* obtained from sampling trajectories of finite-length random walks on the unweighted version of the graph $\widetilde{G}_{\mathcal{M}}$.

Definition 1 (Counterfactual path).

Given a model's predictions $\mathcal{M}(\mathbf{X}) = [\mathcal{M}(\mathbf{x}_1), \dots, \mathcal{M}(\mathbf{x}_n)] \in \{1, \dots, g\}^n$ for a dataset $\mathbf{X} = (\mathbf{x}_1, \dots, \mathbf{x}_n)^T$, we call a sequence $\mathbf{v} = (v_1, \dots, v_k)$, $k \leq p$, a counterfactual path under counterfactual policy Ψ if perturbing (e.g., by permuting) values in the features v_1, \dots, v_k leads to a substantial change in the model's predictions according to the indicator given by Ψ , i.e., if

$$\Psi(\mathcal{M}(\mathbf{X}), \mathcal{M}(\mathbf{X}'_{\mathbf{v}})) = 1.$$

In the above definition, $\mathbf{X}'_{\mathbf{v}}$ represents a dataset with perturbed values of features from the sequence \mathbf{v} (note that perturbations are performed sequentially, for individual variables as they are added to the path). The counterfactual policy Ψ is used to determine whether a permutation of features leads to a significant change in predictions.

Various choices for the counterfactual policy Ψ are possible. One approach is to define Ψ based on the fraction of changed predictions p , where

$$p = \frac{1}{n} \sum_{i=1}^n \mathbb{1}(\mathcal{M}(\mathbf{x}_i) \neq \mathcal{M}(\mathbf{x}'_i)).$$

With that, we define Ψ in a stochastic way as follows:

$$\Psi_s(\mathcal{M}(\mathbf{X}), \mathcal{M}(\mathbf{X}'_{\mathbf{v}})) := X \sim \text{Bern}(p).$$

Alternatively, Ψ can be defined as an indicator of whether the fraction of changed predictions exceeds the selected threshold κ chosen by a user, i.e.,

$$\Psi_d(\mathcal{M}(\mathbf{X}), \mathcal{M}(\mathbf{X}'_{\mathbf{v}})) := \mathbb{1}(p > \kappa).$$

Another option is to penalize path lengths by considering their length k in the definition of Ψ .

The selection of an appropriate counterfactual policy Ψ is a crucial step in the proposed methodology. Once the counterfactual policy is defined, Algorithm 1 is employed to identify and collect counterfactual paths. This algorithm takes several inputs, including the model of interest \mathcal{M} , the dataset \mathbf{X} , the counterfactual policy Ψ , the unweighted graph $\widetilde{G}_{\mathcal{M}}$, the number of iterations n_{iter} , and the maximal path length k . The CPATH algorithm initializes a set to store counterfactual paths and iterates a specified number of times. In each iteration, a new path is generated by sampling vertices from the unweighted graph and checking for significant changes in the model’s predictions based on the counterfactual policy.

Algorithm 1: CPATH: counterfactual paths generation

```

Data:  $\mathcal{M}, \mathbf{X}, \Psi, \widetilde{G}_{\mathcal{M}}, n_{iter} \in \mathbf{Z}_+, k \in \mathbf{Z}_+$ 
1  $CPATHS \leftarrow \{\}$ ;
2 for  $i = 1$  to  $n_{iter}$  do
3    $\mathbf{v} \leftarrow []$ ;
4   for  $j = 1$  to  $k$  do
5      $v_j \leftarrow \text{sample\_vertex}(\widetilde{G}_{\mathcal{M}})$ ;
6      $\mathbf{v} \leftarrow \mathbf{v} + [v_j]$ ;
7     if  $\Psi(\mathcal{M}(\mathbf{X}), \mathcal{M}(\mathbf{X}'_{\mathbf{v}})) = 1$  then
8        $CPATHS \leftarrow CPATHS \cup \{\mathbf{v}\}$ ;
9       break;
10    end
11  end
12 end

```

Subsequently, the observed counterfactual paths are used in Algorithm 2 to estimate the function $w_{\mathcal{M}}$, i.e., derive the corresponding adjacency matrix W . Specifically, the transition matrix \mathbf{T} is calculated by iterating through the generated paths. For each path, the length l of the path is computed. Then, for each consecutive pair of vertices (v_i, v_{i+1}) in the path, the corresponding entry in \mathbf{T} is incremented by $k - l + 1$. This process accounts for the penalization of longer paths, as paths with a shorter length contribute more to the edge weights. The resulting adjacency matrix should capture the underlying dependencies and interactions between variables based on the observed counterfactual paths.

Algorithm 2: CPATH: transition matrix generation

Data: $CPATHS$, $k \in \mathbf{Z}_+$

```

1  $\mathbf{T} \leftarrow \mathbf{0}_{p \times p}$ ;
2 for  $\mathbf{v}$  in  $CPATHS$  do
3    $l \leftarrow \text{length}(\mathbf{v})$ ;
4   if  $l = 1$  then
5      $\mathbf{T}[v_1, v_1] \leftarrow \mathbf{T}[v_1, v_1] + k - l + 1$ ;
6   end
7   for  $i = 1$  to  $l - 1$  do
8      $\mathbf{T}[v_i, v_{i+1}] \leftarrow \mathbf{T}[v_i, v_{i+1}] + k - l + 1$ ;
9   end
10 end

```

Based on the determined adjacency matrix W , we can calculate the importance of individual variables. A straightforward approach is to compute the fraction of weights of edges adjacent to the node corresponding to variable \mathbf{X}_j . This can be expressed as:

$$Imp(\mathbf{X}_j) = \frac{\sum_{i \in [p]} \mathbf{T}[v_i, v_j]}{\sum_{i \in [p], k \in [p]} \mathbf{T}[v_i, v_k]}, \quad (1)$$

where \mathbf{T} is the transition matrix obtained from Algorithm 2 and $[p]$ denotes the set of indices from 1 to p .

Another way to estimate the importance values is by considering the stationary distribution of a Markov chain based on transition matrix \mathbf{P} being the row-wise normalized matrix \mathbf{T} . The stationary distribution represents the long-term probability distribution of being at each node in the graph and it is a vector π that satisfies the condition $\pi \mathbf{P} = \pi$. In this setting, the importance of variable \mathbf{X}_j is given by the corresponding element π_j in the stationary distribution vector.

3.3 Counterfactual paths for causal modeling

In the previous section the transition matrix \mathbf{T} was used to derive feature importances of single features. However, it also contains information about important interactions of features in form of a weighted directed graph. In fact, the generated counterfactual paths in $CPATHS$ can be used for causal modeling and inference, for instance with Bayesian networks. From the absence and presence of features within the detected counterfactual paths one can estimate the conditional probability distribution between the important features, which may help to discovery causal effects. We illustrate this on two concrete examples (section 5: Results).

4 Evaluation and experimental set-up

General approach. We have generated synthetic data under three conditions: Conditional dependency, correlation, and conditional independence (see

Appendix section A.1). For each of these datasets two features were simulated fulfilling the above-mentioned conditions; the rest of the features were added as noise. A Random Forest was trained on synthetic data and predictions were made based on the training set. The model was treated as a black box and explainable methods were exploited to verify the relevant features.

4.1 Explaining the model

The conceptual idea is to compare the feature importance scores computed by the explainers (e.g. SHAP (Aas et al., 2021) and LIME (Ribeiro et al., 2016)) with the model-internal Gini impurity scores generated by the random forest, which we consider here as ground truth. A high correlation between the explainers’ feature importance scores and the model’s Gini impurity scores indicates that the explainers are able to capture the underlying patterns in the model’s behaviour. Here, we report on the correlation with the model-specific Gini impurity scores associated with each simulated feature.

4.2 Explaining the data

We are aware that the Gini impurity scores themselves can be biased due to several shortcomings (Nembrini et al., 2018). As a consequence, we also studied the capability of the explainers to detect the most important features within the data. We could show that the model-specific Gini impurity scores quite efficiently detect the simulated ground truth, which essentially supports the validity of the first evaluation set-up as described above. However, in this particular investigation, the focus was more on the simulated features within the data and not on the features the model actually preferred, which is reflected by our first simulation set-up described above.

In the case of SHAP and LIME, feature importance scores for *global* explanations were computed as the mean absolute values of the local explanation scores. For the data-focused experiment 2) we compared our method also to Conditional Predictive Impact (CPI, Watson and Wright, 2021). CPI provides variable importance measures taking into account the association between one or several features and a given outcome.

4.3 Evaluation of the quality of explanations

There are several methods that are used to measure the quality of explanations; in a survey of surveys (Schwalbe and Finzel, 2023) describe a taxonomy of Explainable AI methods and mention the fundamental differences and commonalities between several quality of explanation metrics. Expressing the expectation of the fact that a substantial change in the model decision’s logic will also be reflected in its explanations is made by the sensitivity metric. Furthermore, fidelity (also referred to as faithfulness) is mainly used in conjecture with a surrogate model (Ancona et al., 2017). It describes the agreement between the original

and surrogate model that is used to provide the explanations. Typically, models strive to have low infidelity, which is computed by the following function:

$$\text{INFD}(\Phi, \mathbf{f}, \mathbf{x}) = \mathbb{E}_{\mathbf{I} \sim \mu_{\mathbf{I}}} \left[\mathbf{I}^T \Phi(\mathbf{f}, \mathbf{x}) - \left(\mathbf{f}(\mathbf{x}) - \mathbf{f}(\mathbf{x} - \mathbf{I}) \right)^2 \right] \quad (2)$$

Equation 2 provides the infidelity for a model computing the function \mathbf{f} , having \mathbf{x} as input. The explanation method is represented by Φ , called “explanation functional”. This metric is based on the definition of suitable perturbations, tailored to the needs of the task, the used model, input and the xAI method. They are represented by the difference $\mathbf{I} = \mathbf{x} - \mathbf{x}_0 \in \mathbb{R}^d$ between the input \mathbf{x} and \mathbf{x}_0 , where \mathbf{x}_0 can be a baseline value, a noisy baseline value or even a Random Variable (RV) (in the equation 2, $\mathbf{I} \sim \mu_{\mathbf{I}}$ is a RV having the probability measure $\mu_{\mathbf{I}}$).

Another metric that is related to infidelity to a certain extent, since it is also based on the principle of using perturbations is sensitivity. In this case, it is not the input data \mathbf{x} that is perturbed but the input features; the perturbation strategy is not defined solely by the data scientist, but it is driven by the relevance/attribution values that each feature has - according to the xAI method of interest. This metric expresses an expectation that the computed attribution values for each feature have some relationship with the computed output of the model. If a feature that is said to be highly important or decisive for a particular prediction is removed or replaced by a less informative one, then this action has to have some impact on the model’s prediction. Even more, this change has to be in some way analogous to the assigned relevance/attribution of the feature, as computed by the xAI method. The extension of sensitivity to subsets of features (and not just one) is called sensitivity- n , where n is the cardinality of the selected feature subset S . The corresponding equation is:

$$\text{Sens}_n = r \left(\sum_{s \in S_i} \mathbf{e}_s, \mathbf{f}(\mathbf{x})_c - \mathbf{f}(\mathbf{x}_{S_i})_c \right) \quad (3)$$

where c is the predicted class, \mathbf{x} is the original input, \mathbf{x}_S is \mathbf{x} with all features in subset S removed. The sum of attributions in the subset S is denoted by $\sum_{s \in S_i} \mathbf{e}_s$ and its Pearson correlation r with the aforementioned difference comprises the value of sensitivity- n . What is questionable is the use of this correlation without considering Spearman’s rank correlation coefficient or Mutual Information (MI) (MacKay, 2003) for capturing non-linear correlations.

A detailed description of the relationship between sensitivity and infidelity for different scenarios is described in (Yeh et al., 2019); the researchers have shown that a small decrease in sensitivity can be achieved when the explanation is multiplied by a smooth kernel (in this case a Gaussian) without increasing the infidelity - and under particular circumstances also decreasing it. This provided a general methodology that can start from any explanation towards one that has more beneficial quality properties - at least as far as those metrics are concerned. A detailed analysis of several related metrics with different representative exper-

iments testing various datasets in the image processing domain is presented in (Gevaert et al., 2022).

4.4 Explanations based on domain knowledge graphs

In the above-described experiments, the counterfactual paths are computed on a fully-connected graph. The domain expert, however, might have some prior knowledge about the functional relationships between the features (nodes in the graph), which could be reflected as edges in a knowledge graph. In these cases, the explanatory factors induced by the counterfactual paths and their visiting nodes can be restricted and guided by domain knowledge.

In this specific evaluation, we compute the network, features and classes in the following way. First, we generate Barabasi networks (Barabási and Albert, 1999) of varying size and structure. Second, we compute the features associated with a node using a normal distribution with $N(\mu = 0, \sigma = 1)$. Following this, we randomly select two connected nodes v_1 and v_2 and apply the following formula.

$$z = 5 * v_1 + 3 * v_2$$

Following, we apply the sigmoid function to transform z in the range between 0 and 1. The formula of the sigmoid function is shown below.

$$S(z) = \frac{1}{1 + e^{-z}}$$

After we get the transformed values from the sigmoid function, we underlay a Bernoulli distribution and sample from it to obtain the outcome class.

In the described experiment the feature sampling in CPATH is guided by the network through random walks. In the remainder of this paper, we refer to it as CPATH_{know}.

Finally, we exemplary show the potential of our approach in a bioinformatics application for biomarker discovery. We used the gene expression data of human breast cancer patient samples for an experimental evaluation of the herein proposed methodologies. The data was retrieved from The Cancer Genome Atlas (TCGA) and was preprocessed as described in (Chereda et al., 2021). We masked the data by the topology of the Human Protein Reference Database (HPRD) protein-protein interaction (PPI) network (Keshava Prasad et al., 2009). The resulting dataset comprised 981 patients and 8469 genes. The binary prediction task was to classify the samples into a group of patients with the luminal A subtype (499 samples) and patients with other breast cancer subtypes (482 samples). Knowledge-guided explanations were generated using CPATH_{know} for the detection of potential breast cancer-specific biomarkers.

5 Results

5.1 Synthetic data: correlation with ground-truth

The correlation with the Gini impurities (herein assumed as the *model-specific ground-truth*) is depicted in Figure 1 and Figure 2. The results indicate that

the path-based explanations are more accurate and especially in the case of conditional feature dependency efficiently reflect the model’s internal behaviour (see Figure 1). In that case, the explanations based on LIME are uninformative. The same observation can be made when interpreting the ability of the methods to detect the relevant features within the data (see Figure 3 and Figure 4). Here, the simulated features are defined as the *data-specific ground-truth*. In the case of conditional feature dependency, CPATH is clearly more accurate than SHAP and LIME. CPATH almost perfectly aligns with the ground truth. CPI outperforms all methods when the signal-to-noise ratio is low. However, there is a substantial performance degradation when this ratio increases. It should be noted that CPI is specially designed for feature selection purposes and not for explaining the internal behaviour of the model. For instance, specialized feature selection methods often use a random forest, e.g. in bioinformatics where both robustness and explainability are important (Pfeifer et al., 2022b) or any other classifier as a wrapper to detect the most relevant features within the data. Robustness and Explainability are necessary to ensure trust in the results (Holzinger, 2021), (Holzinger et al., 2022).

In the case of correlated features CPATH performs slightly worse than the competing SHAP method (see Figure 2). Also Figure 4 suggests that SHAP is the more appropriate explainer in the presence of correlated features. In this data-focused experiment (Figure 4) also LIME is closer to the *ground-truth*. Notably, when the signal-to-noise ratio is high all methods perform almost identically.

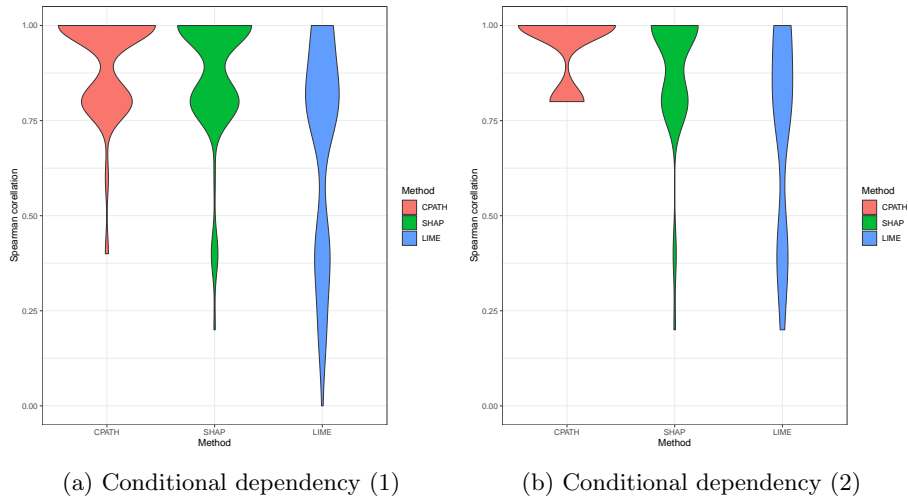


Fig. 1: Spearman correlation with Gini importance values based on 100 simulations.

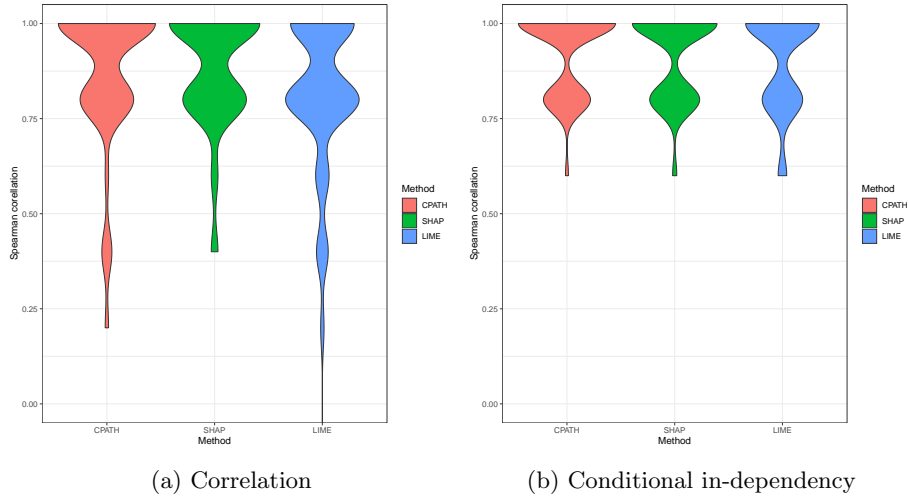


Fig. 2: Spearman correlation with Gini importance values based on 100 simulations.

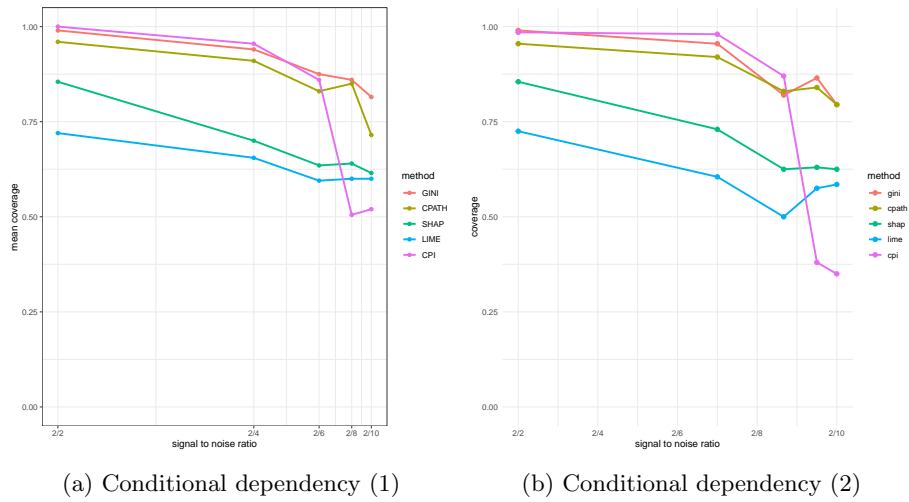


Fig. 3: Mean coverage of important features within the simulated data based on 100 simulations and along the signal-to-noise ratio.

Table 1: Correlation to Gini importances (min/mean/max)

| Experiment | CPATH | SHAP | LIME |
|----------------------------|--------------|-------------|-------------|
| Conditional dependency (1) | 0.4/0.91/1 | 0.2/0.88/1 | 0/0.70/1 |
| Conditional dependency (2) | 0.4/0.90/1 | 0.2/0.90/1 | -0.4/0.69/1 |
| Correlation | 0.2/0.88/1 | 0.4/0.88/1 | -0.4/0.81/1 |
| Conditional in-dependency | 0.6/0.92/1 | 0.6/0.92/1 | 0.6/0.91/1 |

Table 2: Mean coverage of the important features within the data

| Experiment | signal/noise | GINI | CPATH | SHAP | LIME | CPI |
|----------------------------|---------------------|-------------|--------------|-------------|-------------|------------|
| Conditional dependency (1) | 2/2 | 0.990 | 0.960 | 0.855 | 0.720 | 1 |
| Conditional dependency (2) | 2/2 | 0.990 | 0.950 | 0.905 | 0.730 | 0.995 |
| Correlation | 2/2 | 0.995 | 0.960 | 0.905 | 0.725 | 1 |
| Conditional in-dependency | 2/2 | 1 | 1 | 1 | 1 | 1 |
| Conditional dependency (1) | 2/4 | 0.940 | 0.910 | 0.700 | 0.655 | 0.955 |
| Conditional dependency (2) | 2/4 | 0.940 | 0.880 | 0.710 | 0.665 | 0.925 |
| Correlation | 2/4 | 0.760 | 0.700 | 0.705 | 0.770 | 0.805 |
| Conditional in-dependency | 2/4 | 1 | 1 | 1 | 1 | 1 |
| Conditional dependency (1) | 2/6 | 0.875 | 0.830 | 0.635 | 0.595 | 0.860 |
| Conditional dependency (2) | 2/6 | 0.870 | 0.820 | 0.670 | 0.655 | 0.895 |
| Correlation | 2/6 | 0.730 | 0.745 | 0.675 | 0.770 | 0.775 |
| Conditional in-dependency | 2/6 | 1 | 1 | 1 | 1 | 1 |
| Conditional dependency (1) | 2/8 | 0.860 | 0.850 | 0.640 | 0.600 | 0.505 |
| Conditional dependency (2) | 2/8 | 0.845 | 0.805 | 0.615 | 0.600 | 0.400 |
| Correlation | 2/8 | 0.685 | 0.710 | 0.660 | 0.755 | 0.415 |
| Conditional in-dependency | 2/8 | 1 | 1 | 1 | 1 | 0.500 |
| Conditional dependency (1) | 2/10 | 0.815 | 0.715 | 0.615 | 0.600 | 0.520 |
| Conditional dependency (2) | 2/10 | 0.820 | 0.735 | 0.585 | 0.575 | 0.325 |
| Correlation | 2/10 | 0.645 | 0.670 | 0.640 | 0.655 | 0.390 |
| Conditional in-dependency | 2/10 | 0.995 | 0.900 | 0.995 | 0.995 | 0.495 |

5.2 Sensitivity, Infidelity, and Interpretability

We have evaluated the sensitivity and infidelity of the explanations based on four different datasets, namely Ionosphere, Breast Cancer, Diabetes, and Iris. The datasets were retrieved using the R package mlbench (Leisch and Dimitriadou, 2021). We split the data into a train (80%) and test set (20%) and generated explanations based on the test set. In terms of sensitivity, CPATH performs well on all datasets and outperforms LIME and SHAP on two out of four cases (see Appendix Figure 1). LIME in this experiment is the worst-performing method. The fidelity of the explanations based on CPATH is not as good as SHAP, but it is competitive with LIME (see Appendix Figure 2).

To showcase the interpretability of our proposed approach we analyzed the Diabetes dataset in more detail (see Figure 5). The accuracy of the random forest classifier was $AUC = 0.97$. A graphical summary of the generated counterfactual is shown in Figure 5. We can see that the glucose variable causes

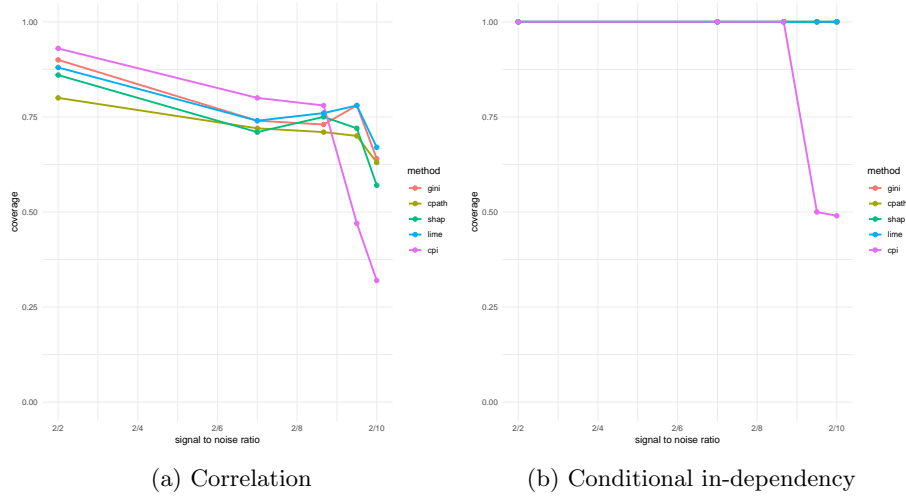


Fig. 4: Mean coverage of important features within the simulated data based on 100 simulations and along a subsequently increased signal-to-noise ratio.

the largest number of swapped labels when it is used as the first node in a counterfactual path. More than 20% labels on average swap when this feature is permuted. Once permuted, insulin and mass increase the swapped fraction up to 30%. However, the largest fraction is obtained by the path starting with pedigree and further going through glucose, mass, and age. This particular path caused > 40% of swapped labels on average. These observations suggest that a combination of the mentioned variables might be a marker for a detailed medical risk assessment. The feature importances derived from the counterfactual paths can be obtained from Figure 6. We further learned a Bayesian network from the inferred counterfactual paths (Figure 6), using the R-package `bnlearn` (Scutari, 2017). While the glucose variable was inferred as the most important feature, the Directed Acyclic Graph (DAG) in Figure 6 (b) indicates that it depends on several features, including age, triceps and insulin, causing the overall importance. From the learned conditional distributions we see that when these features are present within the a given path, it increases the probability of glucose up to 0.72 to be also part of that path, causing the label swap.

5.3 Knowledge-guided explanations and application on Protein-Protein Interaction Network (PPI)

Syntethic Barabasi networks. The experiments on synthetic Barabasi networks indicate that incorporated domain knowledge generates more parsimony and interpretable explanations (see Figure 7). CPATH with incorporated knowledge is more accurate in detecting the relevant features when the path length is low. CPATH without guided domain knowledge requires about three times

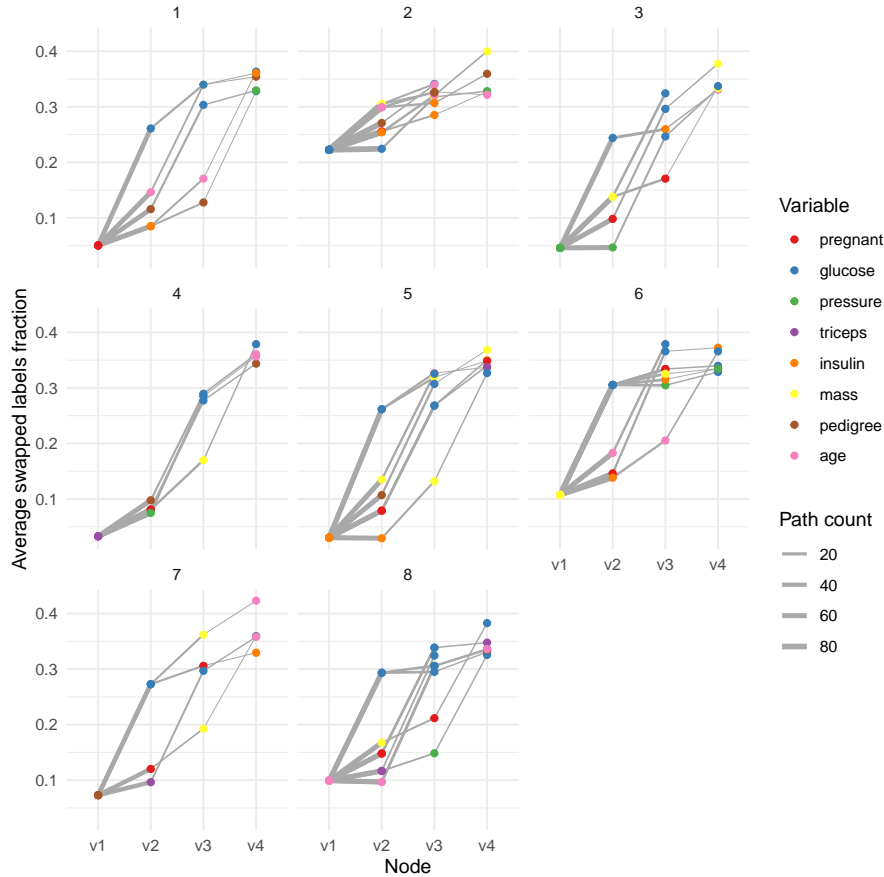


Fig. 5: Diabetes dataset. Graphical summary of the computed counterfactual paths inferred by CPATH.

larger paths to capture the ground truth. Furthermore, knowledge-guided counterfactual explanations converge faster, as indicated by the higher performance when the number of sampled paths is low (Figure 7a). Interestingly, CPATH without domain knowledge significantly outperforms CPATH_{know} when the size of the sampled paths is high. In that case, CPATH is able to explore the feature space more efficiently, while the incorporated knowledge graph seems to hinder optimal convergence. The reason for that behavior is due to the edge degrees of the graph which leads to repeated visits of the same node in a random walk. Thus, we can derive the conclusion that for incorporated knowledge, in the form of a graph, a high number of generated paths is essential to ensure a sufficient number of starting nodes so that the whole graph can be explored by the random walks.

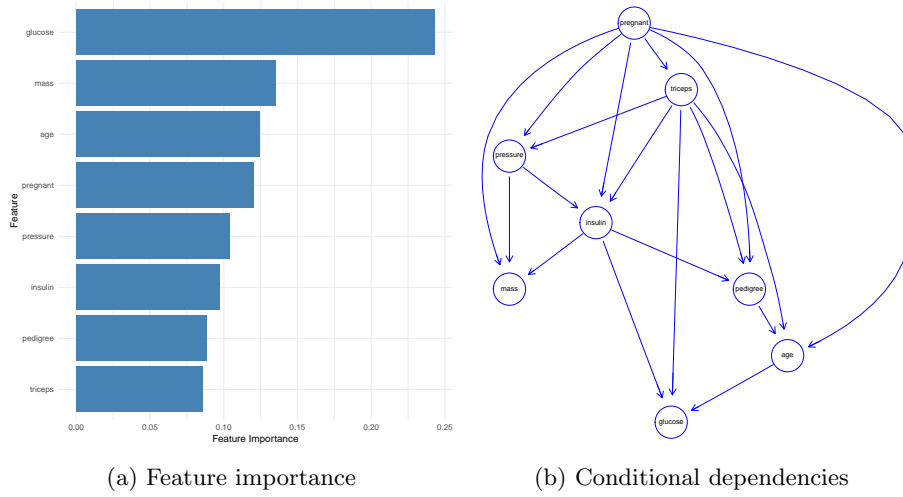


Fig. 6: Diabetes dataset. Feature importances and conditional dependencies inferred by Bayesian network learning and here represented as a Directed Acyclic Graph (DAG).

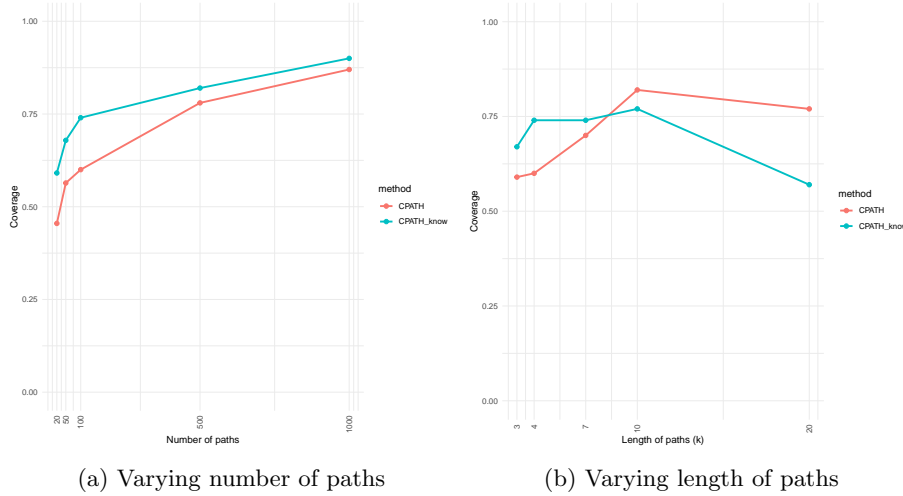


Fig. 7: Mean coverage in detecting the important features within the simulated data, masked by Barabasi networks. The results are based on 100 simulations, where data and network topology are varying. (a) The path length is set to $k = 4$. (b) The number of paths is set to 100.

Application on PPI networks. The retrieved breast cancer data was split into a train (80%) and test set (20%). We trained a random forest comprising 1000 trees and we evaluated the accuracy of the independent hold-out test set. The trained classifier achieved an Area Under the Curve (AUC) of 0.93. Knowledge-guided explanations were generated using *CPATH_know* using a PPI network. We have generated 10000 paths using a path length of $k = 10$. Overall, 118 paths of the generated paths were counterfactuals. The feature importances derived from these paths can be obtained from Figure 8. The top-3 genes were LAT, RANBP1, and KDM5B. Single-feature test set accuracy for these genes were $AUC(LAT)=0.49$, $AUC(RANBP1)=0.73$, and $AUC(KDM5B)=0.54$. These results suggest that LAT and KDM5B on its own are not sufficient as predictive markers.

LAT is a protein that plays a critical role in the immune system and is primarily involved in T cell activation and signaling. It is expressed in T cells and other immune cells, facilitating the transmission of signals from the T cell receptor to the downstream signalling molecules.

The KDM5B gene, also known as JARID1B or PLU-1, is a gene that encodes a protein belonging to the family of histone demethylases. Histone demethylases are enzymes involved in the regulation of gene expression by modifying histone proteins, which are involved in packaging DNA within the nucleus. Studies have implicated KDM5B in various biological processes, including development, differentiation, and cancer. While KDM5B’s role in breast cancer is still being actively investigated, emerging research suggests its involvement in breast cancer progression and metastasis (Di Nisio et al., 2023).

The RANBP1 gene, also known as Ran-binding protein 1, encodes a protein involved in the regulation of the Ran GTPase cycle. The Ran GTPase is essential for nucleocytoplasmic transport, which controls the movement of molecules between the nucleus and the cytoplasm. While RANBP1 itself is not directly associated with breast cancer, aberrant expression or dysregulation of proteins involved in the Ran GTPase cycle, including RANBP1, have been implicated in cancer, including breast cancer (Yuen et al., 2016)(Bamodu et al., 2016). Some studies have suggested that RANBP1 may have tumor suppressor properties. Decreased expression of RANBP1 has been associated with poor prognosis and aggressive features in breast cancer patients. Loss or downregulation of RANBP1 expression may contribute to tumor development and progression.

In a further investigation, we retrieved the first-order neighbourhood (N) of the detected and aforementioned genes. The results were $AUC(N(LAT))=0.78$, $AUC(N(RANBP1))=0.82$, $AUC(N(KDM5B))=0.67$. The neighborhood of the RANBP1 gene ($N(RANBP1)$) included four additional genes, namely RAN, CO93, RCC1, and RANGRF. For this subset, we repeated the generation of *CPATH* explanations, but this time without incorporating domain-knowledge. The number of paths was set to 1000, and the length of paths was $k = 5$. We obtained 864 counterfactual paths. The generated counterfactual paths can be obtained from Figure 9. The shortest counterfactual path goes through RANBB1, RCC1 and RAN, leading to an average of 50% label swaps.

For the first-order neighborhood of RANBP1 we applied bayesian network learning based on the detected counterfactual paths. The RANBP1 strongly depends on the CD93 gene. When CD93 is part of a counterfactual path the probability is 0.74 that RANBP1 also is included.

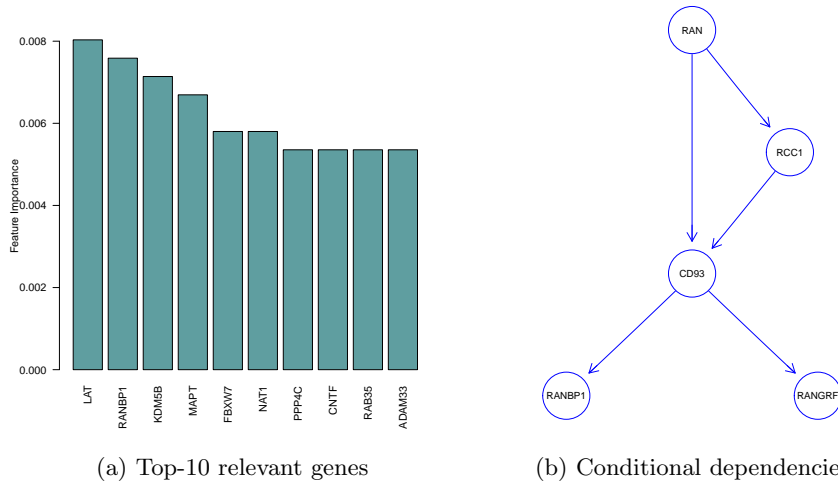


Fig. 8: Breast cancer dataset. (a) Top-10 relevant genes inferred by CPATH with incorporated PPI domain knowledge. (b) Conditional dependencies of the neighborhood features of RANBP1 inferred by Bayesian network learning and here represented by a Directed Acyclic Graph (DAG).

6 Discussion

Apart from the proposed technique, various other approaches can be used to obtain importance values based on sampling trajectories of finite-length random walks on the $\widetilde{G_{\mathcal{M}}}$ graph (with corresponding changes in model predictions). In particular, other approaches can use any sampled trajectory to compute importance scores without relying directly on the definition of counterfactual paths using the counterfactual policy Ψ . Therefore, in our initial experiments, we also tested solutions based on reinforcement learning (RL) methods. The main difference with the technique presented earlier is that in reinforcement learning-based approaches, successive sampled trajectories can be used to update the transition matrix (or directly the importance vector) iteration by iteration, after each episode of the learning process.

When RL techniques are used to estimate feature importance, the agent learns a policy that maximizes the cumulative reward over time. The agent explores the graph by traversing different paths and observing the resulting

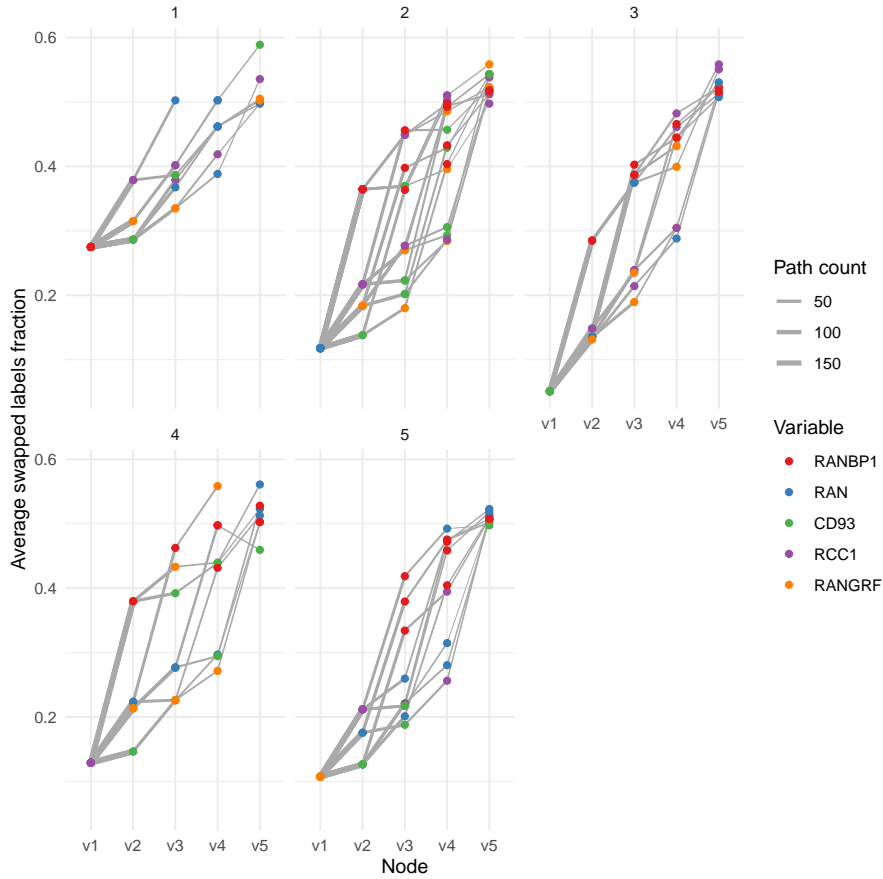


Fig. 9: Breast cancer dataset. Graphical summary of the computed counterfactual paths inferred by CPATH.

changes in the model predictions. Technically, we can formulate the problem as a Markov decision process (MDP), which is a tuple $\langle S, A, P, R \rangle$, where

- S represents the state space corresponding to the set of vertices in the graph $G_{\mathcal{M}}$ (explanatory variables).
- A is the action space, representing the available actions that an RL agent can take in each state. In this case, the actions correspond to traversing from one vertex to another in the graph.
- P denotes the transition probabilities to other states, given the current state and the chosen action. In this particular environment, the state to which an action leads is deterministic (since the action is to select the appropriate edge of the graph).

- R represents the reward function that provides feedback to the RL agent based on its actions. In the context of feature importance, the reward can be defined to reflect the changes in model predictions induced by traversing different paths.

The terminal state is then determined by a fixed maximum number of variables on the path or is associated with exceeding the threshold of the reward (significant change in the model predictions).

In our implementation, a solution using the model-free Q-learning algorithm is available. It estimates the matrix $Q_{p \times p}$ of state-action quality, from which the importance of variables can be extracted by aggregation, analogous to the main method. Other available techniques allow the direct estimation of the state value function (which translates into the importance of the variables) – this can be done using the temporal difference learning TD(0) or the first-visit Monte Carlo algorithm. Although these methods give promising results, they suffer from sensitivity to hyperparameters. They require further research, investigation and validation, which is beyond the scope of this paper.

7 Conclusion

In this work we have presented explainable AI techniques using counterfactual paths. Unlike classical feature importance methods the herein developed methodologies can be efficiently visualized through graphs, which to this end may help to detect important interaction between features and uncover causal effects.

8 Data availability

The herein presented method is implemented within our cpath package (<https://github.com/pievos101/cpath>), available for R and Python.

9 Acknowledgements

Parts of this work have been funded by the Austrian Science Fund (FWF), Project: P-32554 “explainable Artificial Intelligence” (Grantholder AH).

Bibliography

- Aas K, Jullum M, Løland A (2021) Explaining individual predictions when features are dependent: More accurate approximations to shapley values. *Artificial Intelligence* 298:103502
- Alaa AM, Gurdasani D, Harris AL, Rashbass J, van der Schaar M (2021) Machine learning to guide the use of adjuvant therapies for breast cancer. *Nature Machine Intelligence* 3(8):716–726
- Ancona M, Ceolini E, Öztireli C, Gross M (2017) Towards better understanding of gradient-based attribution methods for deep neural networks. arXiv preprint arXiv:171106104
- Au Q, Herbinger J, Stachl C, Bischl B, Casalicchio G (2022) Grouped feature importance and combined features effect plot. *Data Mining and Knowledge Discovery* 36(4):1401–1450
- Bamodu OA, Huang WC, Lee WH, Wu A, Wang LS, Hsiao M, Yeh CT, Chao TY (2016) Aberrant kdm5b expression promotes aggressive breast cancer through malat1 overexpression and downregulation of hsa-mir-448. *BMC cancer* 16:1–18
- Baniecki H, Parzych D, Biecek P (2023) The grammar of interactive explanatory model analysis. *Data Mining and Knowledge Discovery* pp 1–37
- Barabási AL, Albert R (1999) Emergence of scaling in random networks. *science* 286(5439):509–512
- Biecek P, Burzykowski T (2021) *Explanatory Model Analysis*. Chapman and Hall/CRC, New York, URL <https://pbiecek.github.io/ema/>
- Blesch K, Watson DS, Wright MN (2023) Conditional feature importance for mixed data. *AStA Advances in Statistical Analysis* pp 1–20
- Casalicchio G, Molnar C, Bischl B (2019) Visualizing the Feature Importance for Black Box Models. In: *Machine Learning and Knowledge Discovery in Databases*, pp 655–670
- Chereda H, Bleckmann A, Menck K, Perera-Bel J, Stegmaier P, Auer F, Kramer F, Leha A, Beißbarth T (2021) Explaining decisions of graph convolutional neural networks: patient-specific molecular subnetworks responsible for metastasis prediction in breast cancer. *Genome medicine* 13:1–16
- Confalonieri R, Weyde T, Besold TR, Moscoso del Prado Martín F (2021) Using ontologies to enhance human understandability of global post-hoc explanations of black-box models. *Artificial Intelligence* 296:103471
- Covert I, Lundberg SM, Lee SI (2020) Understanding global feature contributions with additive importance measures. *Advances in Neural Information Processing Systems* 33:17212–17223
- Dandl S, Molnar C, Binder M, Bischl B (2020) Multi-Objective Counterfactual Explanations. In: *Parallel Problem Solving from Nature – PPSN XVI*, pp 448–469
- Di Nisio E, Licursi V, Mannironi C, Buglioni V, Paiardini A, Robusti G, Noberini R, Bonaldi T, Negri R (2023) A truncated and catalytically inactive isoform of

- kdm5b histone demethylase accumulates in breast cancer cells and regulates h3k4 tri-methylation and gene expression. *Cancer Gene Therapy* pp 1–11
- Fisher A, Rudin C, Dominici F (2019) All Models are Wrong, but Many are Useful: Learning a Variable’s Importance by Studying an Entire Class of Prediction Models Simultaneously. *Journal of Machine Learning Research* 20(177):1–81
- Gevaert A, Rousseau AJ, Becker T, Valkenburg D, De Bie T, Saeys Y (2022) Evaluating feature attribution methods in the image domain. arXiv preprint arXiv:220212270
- Gosiewska A, Kozak A, Biecek P (2021) Simpler is better: Lifting interpretability-performance trade-off via automated feature engineering. *Decision Support Systems* 150:113556
- Holzinger A (2021) The Next Frontier: AI We Can Really Trust. In: Kamp M (ed) *Proceedings of the ECML PKDD 2021, CCIS 1524*, Springer Nature, pp 427–440
- Holzinger A, Dehmer M, Emmert-Streib F, Cucchiara R, Augenstein I, Del Ser J, Samek W, Jurisica I, Díaz-Rodríguez N (2022) Information fusion as an integrative cross-cutting enabler to achieve robust, explainable, and trustworthy medical artificial intelligence. *Information Fusion* 79(3):263–278
- Karimi AH, Barthe G, Balle B, Valera I (2020) Model-agnostic counterfactual explanations for consequential decisions. In: *International Conference on Artificial Intelligence and Statistics*, pp 895–905
- Keshava Prasad T, Goel R, Kandasamy K, Keerthikumar S, Kumar S, Mathivanan S, Telikicherla D, Raju R, Shafreen B, Venugopal A, et al. (2009) Human protein reference database—2009 update. *Nucleic acids research* 37(suppl_1):D767–D772
- Leisch F, Dimitriadou E (2021) mlbench: Machine Learning Benchmark Problems. R package version 2.1-3.1
- MacKay DJ (2003) *Information theory, inference and learning algorithms*. Cambridge university press
- Molnar C, Freiesleben T, König G, Casalicchio G, Wright MN, Bischl B (2021) Relating the Partial Dependence Plot and Permutation Feature Importance to the Data Generating Process. arXiv preprint arXiv:210901433
- Molnar C, König G, Bischl B, Casalicchio G (2023) Model-agnostic feature importance and effects with dependent features: a conditional subgroup approach. *Data Mining and Knowledge Discovery* pp 1–39
- Mothilal RK, Sharma A, Tan C (2020) Explaining machine learning classifiers through diverse counterfactual explanations. In: *Proceedings of the 2020 Conference on Fairness, Accountability, and Transparency*, pp 607–617
- Nembrini S, König IR, Wright MN (2018) The revival of the gini importance? *Bioinformatics* 34(21):3711–3718
- Panigutti C, Perotti A, Pedreschi D (2020) Doctor XAI: An Ontology-Based Approach to Black-Box Sequential Data Classification Explanations. In: *Proceedings of the 2020 Conference on Fairness, Accountability, and Transparency*, pp 629–639

- Pawelczyk M, Datta T, den Heuvel JV, Kasneci G, Lakkaraju H (2023) Probabilistically Robust Recourse: Navigating the Trade-offs between Costs and Robustness in Algorithmic Recourse. In: The Eleventh International Conference on Learning Representations
- Pfeifer B, Baniecki H, Saranti A, Biecek P, Holzinger A (2022a) Multi-omics disease module detection with an explainable greedy decision forest. *Scientific Reports* 12(1):16857
- Pfeifer B, Holzinger A, Schimek MG (2022b) Robust random forest-based all-relevant feature ranks for trustworthy ai. *Studies in Health Technology and Informatics* 294:137–138
- Ribeiro MT, Singh S, Guestrin C (2016) "why should I trust you?": Explaining the predictions of any classifier. In: Proceedings of the 22nd ACM SIGKDD International Conference on Knowledge Discovery and Data Mining, San Francisco, CA, USA, August 13-17, 2016, pp 1135–1144
- Schwalbe G, Finzel B (2023) A comprehensive taxonomy for explainable artificial intelligence: a systematic survey of surveys on methods and concepts. *Data Mining and Knowledge Discovery* pp 1–59
- Scutari M (2017) Bayesian network constraint-based structure learning algorithms: Parallel and optimized implementations in the bnlearn R package. *Journal of Statistical Software* 77(2):1–20, <https://doi.org/10.18637/jss.v077.i02>
- Wachter S, Mittelstadt B, Russell C (2017) Counterfactual explanations without opening the black box: Automated decisions and the GDPR. *Harv JL & Tech* 31:841
- Watson DS, Wright MN (2021) Testing conditional independence in supervised learning algorithms. *Machine Learning* 110(8):2107–2129
- Yeh CK, Hsieh CY, Suggala A, Inouye DI, Ravikumar PK (2019) On the (in) fidelity and sensitivity of explanations. *Advances in Neural Information Processing Systems* 32
- Yuen HF, Chan KK, Platt-Higgins A, Dakir EH, Matchett KB, Haggag YA, Jithesh PV, Habib T, Faheem A, Dean FA, et al. (2016) Ran gtpase promotes cancer progression via met receptor-mediated downstream signaling. *Oncotarget* 7(46):75854

A Appendix

A.1 Simulation Algorithms

Algorithm 3: Simulation 1. Conditional dependency (1)

```

1  $n = 100, p = 4, D^{n \times p} \sim N(0, 2), y^{n \times 1} \sim Bin(0, 1);$ 
2  $a = 0, b = 0;$ 
3 for  $i = 1$  to  $n$  do
4   if  $D[i, 1] \geq a$  then
5     if  $D[i, 2] \geq b$  then
6        $y[i] = 1;$ 
7     end
8   else
9     if  $D[i, 2] \geq b$  then
10       $y[i] = 0;$ 
11    end
12  end
13 end

```

Algorithm 4: Simulation 2. Conditional dependency (2)

```

1  $n = 100, p = 4, D^{n \times p} \sim N(0, 2), y^{n \times 1} \sim Bin(0, 1);$ 
2  $a = 0, b = 0;$ 
3 for  $i = 1$  to  $n$  do
4   if  $D[i, 1] \geq a$  then
5     if  $D[i, 2] \leq b$  then
6        $y[i] = 1;$ 
7     else
8        $y[i] = 0;$ 
9     end
10  end
11 end

```

Algorithm 5: Simulation 3. Correlation

```

1  $n = 100, p = 4, D^{n \times p} \sim N(0, 2), y^{n \times 1} \sim Bin(0, 1);$ 
2  $a = 0;$ 
3 for  $i = 1$  to  $n$  do
4   if  $D[i, 1] \geq a \ \& \ D[i, 2] \geq a$  then
5      $y[i] = 1;$ 
6   end
7 end

```

Algorithm 6: Simulation 4. Conditional in-dependency

```
1  $n = 100, p = 4, D^{n \times p} \sim N(0, 2), y^{n \times 1} \sim Bin(0, 1)$ ;
2  $a = 0$ ;
3 for  $i = 1$  to  $n$  do
4   if  $D[i, 1] \geq a$  &  $D[i, 2] \geq a$  then
5     | next;
6   end
7   if  $D[i, 1] \geq a$  then
8     |  $y[i] = 1$ ;
9   end
10  if  $D[i, 2] \geq a$  then
11    |  $y[i] = 0$ ;
12  end
13 end
```

A.2 Supporting Figures

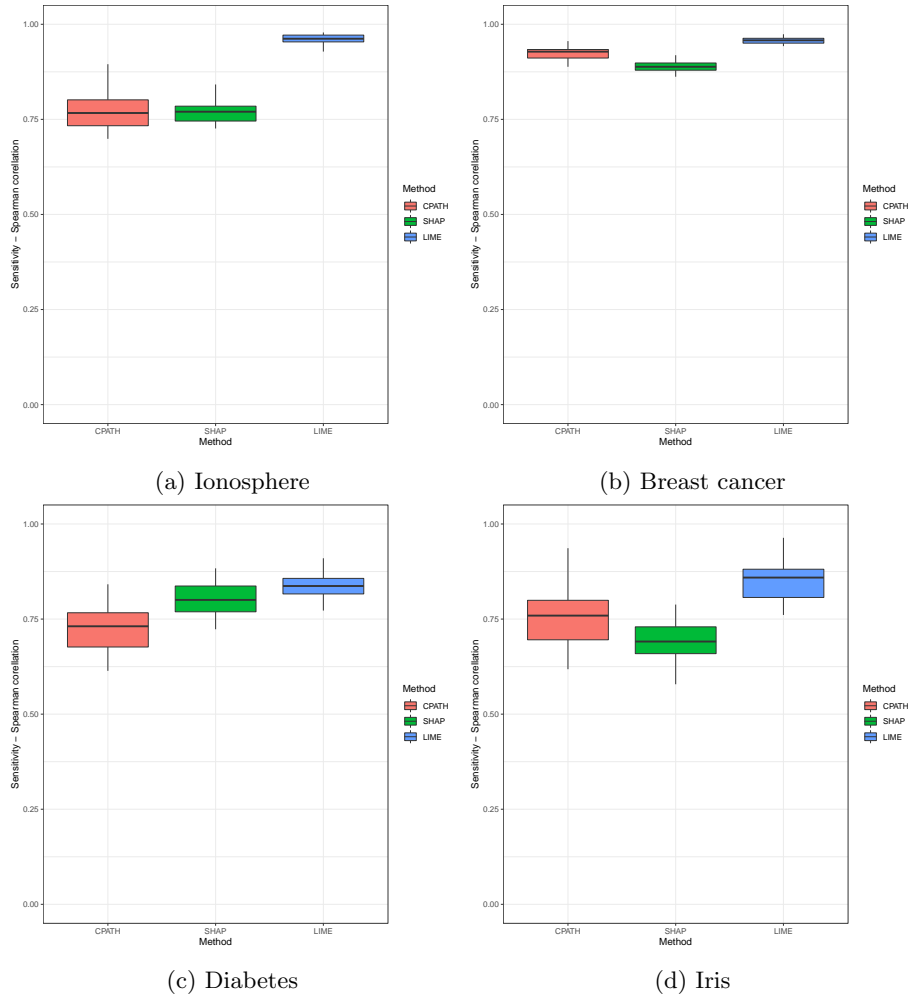
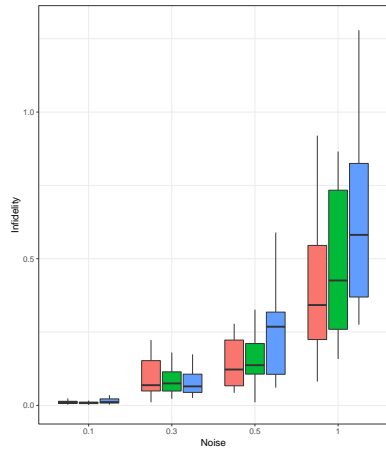
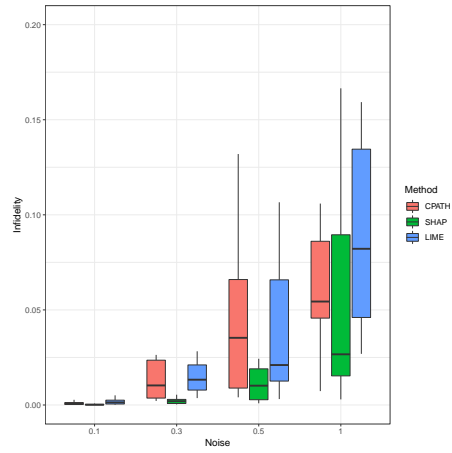


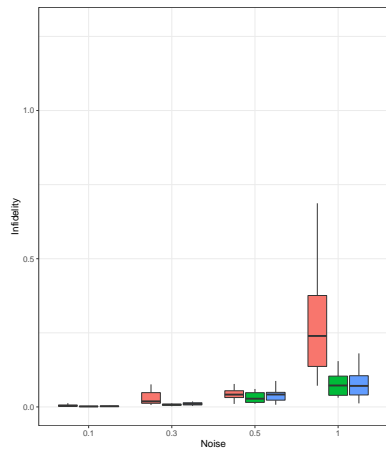
Fig. Appendix Figure 1: Sensitivity



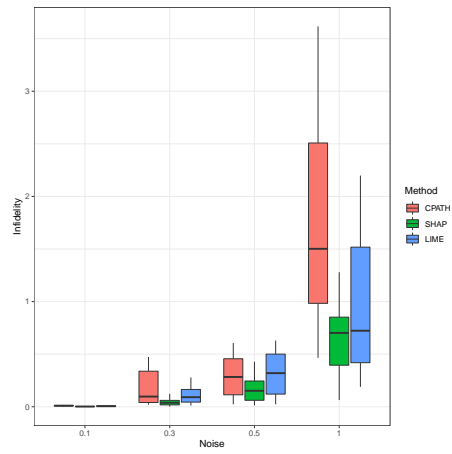
(a) Ionosphere



(b) Breast cancer



(c) Diabetes



(d) Iris

Fig. Appendix Figure 2: Infidelity